# Lattice-matched multiple channel AlScN/GaN heterostructures

View Online　　Export Citation　　CrossMark

Thai-Son Nguyen,[1,a] (iD) Naomi Pieczulewski,[1] (iD) Chandrashekhar Savant,[1] (iD) Joshua J. P. Cooper,[2] (iD)
Joseph Casamento,[3] (iD) Rachel S. Goldman,[2] (iD) David A. Muller,[4,5] (iD) Huili G. Xing,[1,4,6] (iD)
and Debdeep Jena[1,4,6] (iD)

## AFFILIATIONS

[1] Department of Materials Science and Engineering, Cornell University, Ithaca, New York 14853, USA
[2] Department of Materials Science and Engineering, University of Michigan, Ann Arbor, Michigan 48109, USA
[3] Department of Materials Science and Engineering, Massachusetts Institute of Technology, Cambridge, Massachusetts 02139, USA
[4] Kavli Institute at Cornell for Nanoscale Science, Cornell University, Ithaca, New York 14853, USA
[5] School of Applied and Engineering Physics, Cornell University, Ithaca, New York 14853, USA
[6] Department of Electrical and Computer Engineering, Cornell University, Ithaca, New York 14853, USA

[a] Author to whom correspondence should be addressed: tn354@cornell.edu

## ABSTRACT

AlScN is a new wide bandgap, high-k, ferroelectric material for radio frequency (RF), memory, and power applications. Successful integration of high-quality AlScN with GaN in epitaxial layer stacks depends strongly on the ability to control lattice parameters and surface or interface through growth. This study investigates the molecular beam epitaxy growth and transport properties of AlScN/GaN multilayer heterostructures. Single-layer $Al_{1-x}Sc_xN$/GaN heterostructures exhibited lattice-matched composition within $x = 0.09–0.11$ using substrate (thermocouple) growth temperatures between 330 and 630 °C. By targeting the lattice-matched Sc composition, pseudomorphic AlScN/GaN multilayer structures with ten and twenty periods were achieved, exhibiting excellent structural and interface properties as confirmed by x-ray diffraction (XRD) and scanning transmission electron microscopy (STEM). These multilayer heterostructures exhibited substantial polarization-induced net mobile charge densities of up to $8.24 \times 10^{14}$/cm$^2$ for twenty channels. The sheet density scales with the number of AlScN/GaN periods. By identifying lattice-matched growth condition and using it to generate multiple conductive channels, this work enhances our understanding of the AlScN/GaN material platform.

## I. INTRODUCTION

Aluminum scandium nitride (AlScN) is an emerging group III nitride material that has received significant research interest in the past decade. The addition of Sc into AlN was first reported to drastically increase the piezoelectric coefficients of AlScN alloy compared to the highly piezoelectric AlN.[1,2] More recently, reactive sputtered and plasma-assisted molecular beam epitaxy (PA-MBE) AlScN films have been reported to be the first ferroelectric III-nitride material.[3–8] AlScN also shows high potential in nonlinear optics[9] and distributed Bragg reflectors.[10] These properties of AlScN add new functionalities by device integration with both III-nitride semiconductors, and with silicon CMOS where it is already in use in commercial BAW filters.

While the growth, structural, electrical, and piezoelectric properties of single-layer AlScN thin films have been extensively studied, the integration of AlScN multilayers remains unexplored. Multilayers of binary, ternary, and quaternary alloys in group III-arsenides and in group III-nitrides have enabled various electronic and photonic device applications, such as multichannel high-electron mobility transistors (HEMTs), resonant tunneling diodes, solar cells, laser diodes, and infrared emitters and detectors. In the III-As material

family, lattice-matched (Al,Ga)As alloys allowed for the development of single- and multi-layer heterostructures, such as multiple quantum wells and superlattices with low dislocation density and excellent interfaces,[11] which enabled device technologies such as superlattice-castellated field-effect transistors (SLCFETs)[12] and quantum cascade lasers.[13]

Lattice-matched group III-nitride heterostructures are limited due to the 2.6% in-plane lattice mismatch of AlN–GaN and 13% lattice mismatch of AlN–InN. $Al_{0.82}In_{0.18}N$/GaN is the only known lattice-matched ternary–binary pair and can be difficult to grow due to the large growth temperature mismatch between InN and AlN. Using Al(Ga,In)N/GaN multilayer structures, GaN-based resonant tunneling diodes,[14] distributed Bragg reflectors,[15] quantum cascade lasers,[16] multichannel HEMTs for high-power electronic, and RF switches[12,17] have been realized. However, structural degradation due to strain relaxation[18] and complex strain engineering of Al(Ga)N/GaN superlattices[19,20] pose intrinsic limitations in such multilayers.

AlScN is a promising candidate to help overcome these limitations because (1) lattice-matching of AlScN to GaN is theoretically predicted and experimentally demonstrated to be possible;[10,21–23] (2) AlScN has a large growth temperature window that is compatible with GaN epitaxy,[24–27] making it compatible with both CMOS- and GaN-based growth requirements; and (3) AlScN offers strong spontaneous polarization,[2,28] high refractive index mismatch to GaN,[10,26,29] and compressive or tensile strain compositions for flexible bandgap, refractive index, and strain engineering.

The growth and characterization of AlScN/GaN multilayer heterostructures have been studied by a few groups recently. Dzuba *et al.* examined epitaxial AlScN/GaN multiple quantum well heterostructures with quantum well thicknesses below 10 nm to study near-infrared intersubband absorption.[30] Lattice-matched AlScN/GaN multilayer heterostructures were demonstrated as a highly reflective distributed Bragg reflector.[10] However, the lattice-matched composition of AlScN on GaN has been reported to range from 9% to 20% Sc.[22,24,25,27,30–33] Finding the correct lattice-matched composition of AlScN on GaN and its dependence on growth methods and conditions is critical to realize high-quality AlScN/GaN multilayer structures.

This work aims to (1) identify and use the correct Sc composition for lattice-matched AlScN on GaN, (2) realize lattice-matched AlScN/GaN multilayer heterostructures, and (3) study polarization-induced charges in these multilayers. To achieve these goals, (1) we grew AlScN thin films of 80–100 nm thickness on bulk GaN substrates. By varying the Sc composition and growth temperature, we find the lattice-matched composition of MBE AlScN on GaN to be between 9% and 11% Sc composition. (2) Using the single-layer lattice-matched condition, we demonstrate pseudomorphic AlScN/GaN multilayer heterostructures on semi-insulating GaN substrates that exhibit high crystalline and interface quality as we verify by x-ray diffraction (XRD) and scanning transmission electron microscopy (STEM). We measure an in-plane lattice mismatch of 0.02% between AlScN and GaN epilayers in a ten-period 12% Sc AlScN/GaN sample. (3) These pseudomorphic multilayer AlScN/GaN heterostructures were observed to house extremely high mobile carrier densities exceeding $8 \times 10^{14}$/cm² for twenty 2DEG channels. The sheet carrier density was seen to scale linearly with the number of repeating AlScN/GaN periods.

## II. METHODS

We grew AlScN single-layer and multilayer heterostructures in a Veeco GenXplor MBE reactor. Scandium (99.9% purity, Ames Laboratory), aluminum (99.9999% purity), gallium (99.999 99% purity), and silicon (99.999 99% purity) were supplied using Knudsen effusion cells. We used a RF plasma source with a nitrogen flow rate of 1.95 sccm and 200 W RF power to provide active nitrogen species. We monitored thin film growth *in situ* using a KSA Instruments reflection high-energy electron diffraction (RHEED) apparatus with a Staib electron gun operating at 15 kV and 1.5 A. The growth temperatures were measured by a thermocouple on the backside of the substrate. We used bulk silicon-doped Ga-polar n-type GaN ($n^+$GaN) from Ammono for single-layer AlScN growths and bulk semi-insulating GaN substrate from Ammono for multilayer AlScN/GaN growth to evaluate the transport properties of mobile charges in this heterostructure. All the substrates were c-plane and Ga-polar, yielding c-oriented, metal-polar MBE GaN and AlScN films.

We grew AlScN films under nitrogen-rich conditions with a metal (Sc+Al) to nitrogen (III/V) ratio of 0.7 to achieve wurtzite phase AlScN.[24–26,34] We employed metal-rich conditions for GaN epitaxy to promote step-flow growth mode. The beam equivalent pressures (BEPs) of Sc, Al, and Ga used were $\sim 1.5 \times 10^{-8}$, $\sim 1 \times 10^{-7}$, and $\sim 6 \times 10^{-7}$ Torr, respectively. The growth rates of AlScN and GaN were 3.0 and 3.8 nm/min, respectively.

To explore the effect of Sc composition on the structural properties of AlScN films, we grew 80–100 nm thick AlScN films on 100 nm Si-doped $n^+$GaN buffer layer on bulk $n^+$GaN substrates. Since the critical thickness of AlScN on GaN is affected by Sc composition and strain relaxation, only films within ±1.3% Sc composition from the lattice-matched composition can remain coherently strained for AlScN thicknesses between 80 and 100 nm,[21,35] limiting false identification of strained films as the lattice-matched compositions. Unless otherwise noted, we grew single-layer AlScN films at 530 °C and $n^+$GaN buffer layers at 630 °C.

We grew one ten-period and one twenty-period 45 nm AlScN/40 nm GaN multilayer structure on bulk semi-insulating GaN to evaluate the structural qualities of multilayer AlScN/GaN heterostructures with thick AlScN/GaN periods, using the same III/V ratios of $\sim$ 1 and 0.7 for GaN and AlScN, respectively, and a substrate thermocouple temperature of 530 °C. Similar heterostructures with the same AlScN and GaN thicknesses have demonstrated high reflectivity as distributed Bragg reflectors.[10] All the layers were grown at 530 °C substrate thermocouple temperature. We fully desorbed excess Ga in the GaN epilayers before growing subsequent AlScN layers to prevent Ga incorporation during the nitrogen-rich AlScN growth.

A PANalytical Empyrean system with Cu $K_{\alpha 1}$ radiation was used for x-ray diffraction (XRD) and reciprocal space mapping (RSM). We characterized the surface morphology using an Asylum Research Cypher ES atomic force microscope (AFM). To determine the scandium composition, we employed energy-dispersive x-ray spectroscopy using a Zeiss LEO 1550 FESEM equipped with a Bruker energy dispersive x-ray spectroscopy (EDS) silicon drift detector (SDD), X-ray photoelectron spectroscopy (XPS) using a Scienta Omicron ESCA-2SR XPS instrument equipped with a 1486.6 eV Al K$\alpha$, and Rutherford backscattering spectrometry (RBS) at the Michigan Ion Beam Laboratory using 2 MeV $\alpha$ particles generated

in a General Ionex tandem accelerator with backscattered $\alpha$ particles detected by using a silicon surface-barrier detector located at 170° with respect to the incident beam. We used a standard Van der Pauw geometry and a Nanometrics Hall HL5500 system with a magnetic field of 0.325 T to measure the transport properties of AlScN/GaN multilayers at room temperature. We prepared cross-sectional STEM samples using a Thermo Fisher Helios G4 UX focused ion beam with a final milling step of 5 keV and carried out STEM measurements using an aberration-corrected Thermo Fisher Spectra 300 CFEG operated at 300 keV. Secondary ion mass spectrometry (SIMS) measurement was performed by the Eurofins Evans Analytical Group (EAG).

## III. RESULTS AND DISCUSSION

Figure 1(a) shows the layer structure of $Al_{1-x}Sc_xN$ films of thickness 80–100 nm grown on bulk $n^+$ GaN substrates to determine the Sc content $x$ that satisfies the lattice-matching condition to GaN, and to explore the crystal quality and surface morphology as $x$ is varied. We chose this thickness range to achieve relaxed films on the bulk nGaN substrate. Figure 1(b) shows a typical *in situ* RHEED pattern along the ⟨110⟩ zone axis after AlScN growth. The spot-modulated streak pattern suggests a mixed growth mode in which island-like surface features are promoted due to the N-rich growth condition. Figure 1(c) shows a typical $2 \times 2$ $\mu m^2$ post-growth surface morphology measured by AFM, with reasonably smooth root

mean square (rms) roughness of 0.5–1 nm. The surface is dominated by 30–50 nm diameter island features, consistent with the RHEED pattern and other reports on N-rich growth of AlScN.[25,34] Figure 1(d) shows symmetric $2\theta$-$\omega$ scans that confirm the wurtzite phase with strong c-axis orientation of AlScN films via the strong (0002) AlScN diffraction peak near $2\theta = 36°$. The shift from high to low to high $2\theta$ peak values depicts the non-monotonic dependence of the out-of-plane $c$ lattice parameter with Sc composition.

The non-monotonic change of the AlScN peak with Sc content $x$ indicated by arrows was reported in previous studies.[24,25] It is attributed to the distorted bond angles and lengths in the $(Al,Sc)N_4$ tetrahedra.[36] This non-monotonic trend also suggests that there are *two* alloy compositions between 9% and 15% Sc that match the out-of-plane $c$ lattice parameter of AlN, indicating the potential for future integration of non-polar epitaxial AlScN in m-plane and a-plane AlN-based photonic devices.[37] The crystalline wurtzite phase can be maintained to $\sim x = 0.3$, or 30% Sc with interference fringes shown in Fig. 1(d) for some compositions, indicating that highly smooth AlScN-GaN interface can be achieved over a broad range of Sc compositions. Notably, the AlScN (0002) peak with more than five satellite Pendellösung fringes on each side and strongest relative fringe intensity were observed in samples with $x \approx 0.11$–$0.12$, suggesting the highest interface quality between AlScN and $n^+$ GaN layers achieved near these compositions.

To accurately determine the Sc content in the AlScN films, we used the complementary experimental techniques of RBS, EDS, XPS, and SIMS. Of these techniques, RBS, EDS, and SIMS provide thin film composition information, while XPS provides surface composition information. We first measured three samples over a broad range of Sc composition (5%–25%) by RBS, EDS, and XPS, with RBS compositions serving as the standard. Sc compositions were determined from RBS yield vs energy spectra, with $\alpha$ backscattered from Sc detected at energies between 1.3 and 1.45 MeV. Analysis of the RBS data was conducted using the simulation of nuclear reaction analysis (SIMNRA) software. For XPS, a hemispherical capacitor analyzer was used to collect the photoelectrons to obtain high-resolution Al 2p, Sc 3s, Sc 2p, and N 1s spectra. For EDS, the Al K$\alpha$ and Sc K$\alpha$ peaks were used to determine the Sc composition. It is important to use a standard-less method such as RBS to calibrate EDS, sensitive to accelerating voltage conditions, and XPS, sensitive to relative sensitivity factors and surface impurity.

Figure 2 shows EDS and XPS Sc compositions plotted against the RBS compositions for three samples with Sc compositions of $4.7 \pm 1.2\%$ Sc, $10.1 \pm 1.5\%$, and $24.4 \pm 1.8\%$ Sc measured by RBS. The same samples measured by EDS at 12 kV (XPS) showed Sc compositions of $4.5 \pm 0.2\%$ ($4.3 \pm 0.4\%$), $10.3 \pm 0.1\%$ ($10.3 \pm 0.6\%$), and $24.3 \pm 0.3\%$ ($24.5 \pm 0.3\%$) Sc composition, demonstrating good agreement with the RBS composition. The EDS and XPS Sc compositions of eight additional AlScN samples without RBS data also showed a good correlation between EDS and XPS compositions and closely tracked the RBS linear-fit (dashed line), suggesting the reliability of both methods after calibration. Because EDS is less sensitive to surface contamination than XPS and less time-consuming than RBS and SIMS, it is the method of choice in most $Al_{1-x}Sc_xN$ studies to date with the uncertainty of $x \sim \pm 0.01$, or 1%.[3,22,26] Unless otherwise noted, the Sc compositions reported in this work were determined by EDS with an expected uncertainty of ±1.5% Sc mainly due to the RBS uncertainty.
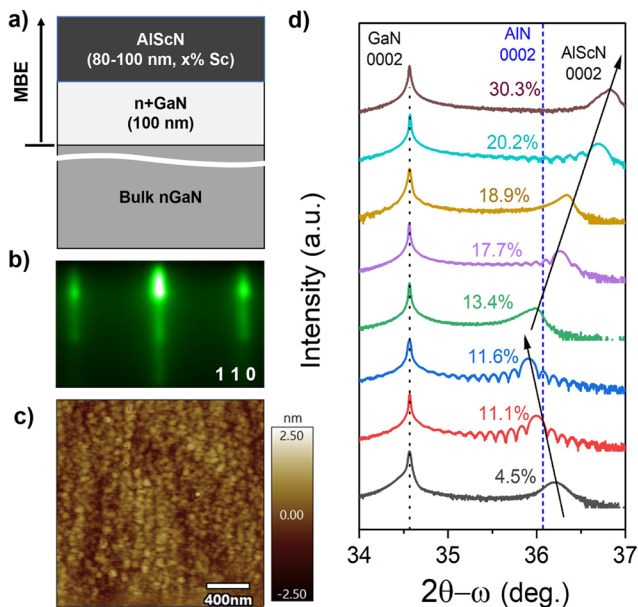


**FIG. 1.** (a) Single-layer AlScN films with thickness of around 100 nm and varying Sc compositions were grown on a bulk n-type GaN substrate. (b) Typical RHEED pattern of an AlScN layer grown under nitrogen-rich conditions showing spot-modulated streak patterns. (c) A typical $2 \times 2$ $\mu m^2$ AFM micrograph of a 100 nm AlScN layer with rms roughness below 1 nm. (d) Symmetric $2\theta$-$\omega$ XRD scans depict the non-monotononic change in the c-parameter of AlScN with Sc composition.
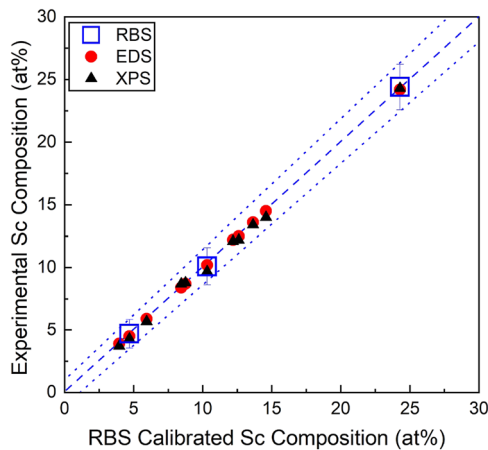
**FIG. 2.** Sc content in single-layer AlScN films measured by Rutherford backscattering spectrometry (RBS), energy dispersive x-ray spectroscopy (EDS), and x-ray photoelectron spectroscopy (XPS). Three samples were measured by RBS, a standard-less method and served as calibration standards for EDS and XPS. The RBS measurement uncertainty is shown for reference. The Sc compositions measured in eight additional samples by XPS and EDS closely follow the RBS linear-fit (dashed line). The dotted lines show the ±1.5% range of uncertainty based on the RBS measurements.

Next, we examined the in-plane lattice constant $a$, out-of-plane lattice constant $c$, and the $c/a$ ratio of $Al_{1-x}Sc_xN$ samples grown at 530 °C using RSM, as shown in Fig. 3. Figure 3(a) shows that $a$ increases monotonically with increasing Sc composition. As highlighted by the gray box shown in Fig. 3(a), $a_{AlScN} \approx a_{GaN} = 3.189$ Å for $x \sim 0.09–0.11$ and strain relaxation occurs outside this range, as suggested by RSM (supplementary material, Fig. S1). These near lattice-matched compositions correspond well with the samples that exhibited strong thickness fringes in symmetric $2\theta$-$\omega$ scans shown in Fig. 1(d). Linear fitting of the $a$ parameter data in this work with Sc composition yielded $a = 3.13 + 0.636x$, where $x$ is the Sc mole

fraction in $Al_{1-x}Sc_xN$, suggesting a lattice-matched composition of 9.4 ± 1.5% Sc. Figure 3(b) shows the AlScN out-of-plane lattice constant $c$ vs Sc content. For $0 \le x \le 0.08$ and $0.13 \le x \le 0.30$, $c$ decreases with increasing Sc composition. However, $c$ increases quickly for $0.08 < x < 0.13$, in accordance with the non-monotonic trend observed in the symmetric $2\theta$-$\omega$ scans [Fig. 1(d)]. Notably, this increase in $c$ corresponds directly to the compositions around which $a_{AlScN} \approx a_{GaN}$, i.e., the lattice-matched composition.

While the non-monotononic change in $c$ with Sc composition is mainly attributed to AlScN tetrahedron distortion, the strong correlation between the increase in $c$ and the near-lattice-matched compositions observed here suggests a contribution from the Poisson's ratio of the thin film near the lattice-matched composition. With increasing Sc content, a pseudomorphic AlScN film becomes more compressively strained in the in-plane direction and tensilely strained in the out-of-plane direction, therefore, causing the $c$ parameter to increase with Sc%. The $c/a$ ratio in Fig. 3(c) also shows a monotonically decreasing trend, except between $x = 0.09$ and $x = 0.11$, i.e., the near lattice-matched compositions.

It is important to note that previous studies have reported several lattice-matched Sc compositions ranging from 9% to 20% Sc.[22,24,25,30–32] We see in Fig. 3 that MBE AlScN films have a more drastic increase in $a$, decrease in $c$, and decrease in $c/a$ ratio compared to sputtered AlScN films. This observation can have strong implications on the difference in the wurtzite-rocksalt transition boundary, structural and piezoelectric properties, and ferroelectric properties of MBE and sputtered AlScN.[1,3,4,38] AlScN film thickness can affect the measured in-plane lattice parameter due to strain relaxation. The lattice-matched composition between 9% and 11% Sc determined from Fig. 3 is in good agreement with the report by Dinh et al. of 9% Sc lattice-matched composition of MBE-grown AlScN.[22] Moreover, the change in $a$ and $c$ constants and $c/a$ ratio observed in this work also aligns with the values reported by Dinh et al. for up to $x = 0.15$,[22] demonstrating the similarities in these MBE AlScN thin films. On the other hand, in recent studies on MBE AlScN films, Motoki et al.[27] and Kumar et al.[33] suggested the lattice-matched Sc composition of 12% by fitting the reported in-plane
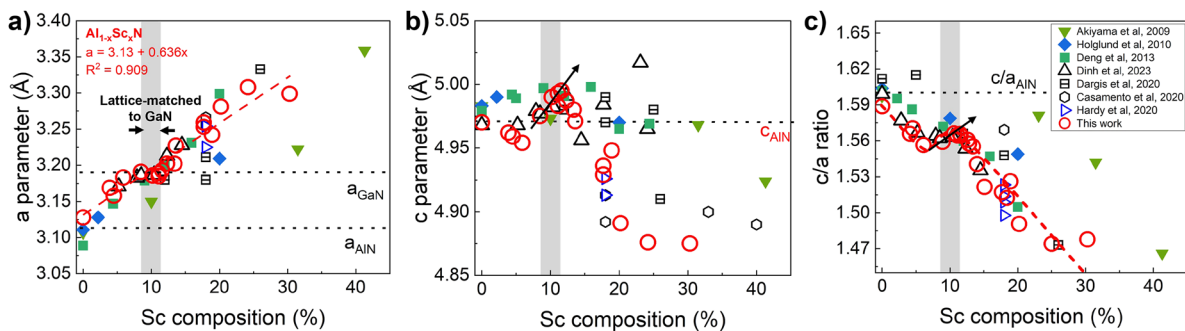


**FIG. 3.** Lattice parameters of $Al_{1-x}Sc_xN$ samples grown at 530 °C vs Sc composition obtained from RSM scans (hollow red circles) compared to values reported in previous studies with AlScN grown by MBE (hollow)[22,24,25,32] and reactive sputtering (solid).[1,23,31] (a) AlScN in-plane lattice parameter $a$ increases monotonically with increasing Sc composition, showing clear strain relaxation outside 9%–11% Sc. The linear fit equation was performed on the data from this work (red circles). (b) AlScN out-of-plane lattice parameter c vs Sc composition. The gray stripe highlights how the c-parameter increases with the Sc content around the lattice-matched composition. (c) $c/a$ ratio shows a monotonically decreasing trend except between 9% and 11% Sc. The dashed line (a) and the arrows (b) and (c) are added as guides to the eye. The results in this study align most closely with the data from Dinh et al.[22]

lattice constant $a$ in the literature and 14% by RSM analysis, respectively. The difference in growth temperature, ranging from 550 °C[33] to 700 °C,[22] could impact the lattice constants[30] and, therefore, the lattice-matched composition. Recent studies also reported Sc atomic segregation in both MBE[30,39] and sputtered[5] AlScN. Atomic segregation can induce local variation of lattice constants to different extents, impacting the lattice-matched composition. One variable of MBE growth not examined in this work is the effect of III/V ratio on structural properties, which could affect the lattice parameters and surface morphology of AlScN.[34] Nevertheless, the wide variation in reported lattice-matched composition means that careful calibrations are needed to determine the correct lattice-matched Sc content depending on growth techniques and conditions.

Figure 4 shows the effect of growth temperature on the structural properties of single-layer, 100 nm AlScN thin films grown on a bulk n⁺GaN substrate. Both Hardy *et al.* and Dzuba *et al.* reported a strong dependence of lattice constants on growth temperature.[24,30] Here, we grew AlScN with three different Sc compositions (9%, 13%, and 19%) under nominally similar conditions and changed the substrate temperature between 330 and 630 °C. Figures 4(a) and 4(b) show the change in $a$ and $c$ with respect to growth temperature, respectively. From Fig. 4(a), we see that the 9% Sc AlScN films were almost pseudomorphically grown on GaN with no change in the $a$ parameter as a function of substrate temperature. On the other hand, the 19% Sc containing AlScN samples are fully relaxed, exhibiting ~1.5% in-plane lattice mismatch compared to GaN. Notably, the $a$ lattice constant exhibited a strong temperature

dependence in 13% samples. For $T_{sub}$ = 330 and 430 °C, the 13% Sc AlScN films were nearly fully strained to GaN, i.e., $a_{AlScN}$ ~ 3.19 Å. However, $a$ quickly increased with increasing substrate temperature, approaching $a_{AlScN}$ ~ 3.23 Å for $T_{sub}$ = 630 °C. This increase is induced by the elevated effects of strain relaxation at higher growth temperatures. Therefore, Fig. 4(a) further corroborates the lattice-matched composition to be near 9%–11% Sc. Interestingly, the $a$ lattice parameter of the 9% Sc AlScN film is nearly equal to the $a$ lattice parameter of GaN [Fig. 4(a)], whereas the $c$ lattice parameter of the 9% Sc AlScN film is nearly equal to the $c$ lattice parameter of AlN [Fig. 4(b)], suggesting the ability to lattice match 9% Sc AlScN to c-plane GaN or m-plane AlN.

It is interesting to note from Fig. 4(a) that while the $c$ parameter of 9% samples is not strongly dependent on the growth temperature, the $c$ parameter of the relaxed 19% samples decreases sharply with increasing growth temperature, suggesting a decrease in unit cell volume with increasing growth temperature. The same decrease in the $c$ parameter with increasing growth temperature was also reported by Wang *et al.* for 50–100 nm MBE 20% Sc AlScN[26] and by Dzuba *et al.* for 40 nm MBE 14% and 18% Sc AlScN films.[30] Both studies attributed this effect to residual strain induced by different growth temperatures, again suggesting that the lattice-matched composition is lower than 18% Sc. Figure 4(c) shows the change in surface morphology of AlScN thin films with Sc composition and growth temperature. For nearly pseudomorphic AlScN on GaN samples, the AFM surface morphology showed larger but smoother islands that could follow the underlying GaN atomic steps and the
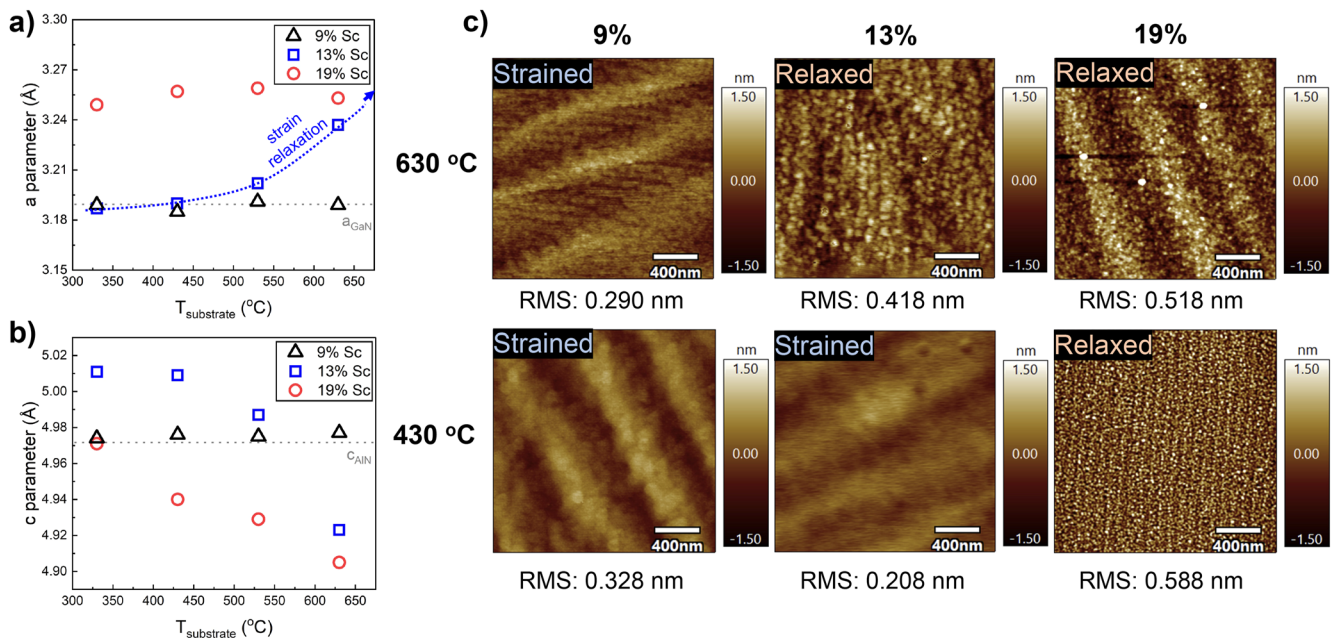


**FIG. 4.** (a) AlScN in-plane a-parameter and (b) out-of-plane c-parameter as a function of growth temperature. Similar Sc composition and III/V ratio were used. The a-parameter of 13% Sc films increases quickly with temperature due to thermally induced strain relaxation at higher growth temperatures. (c) 2 × 2 $\mu$m² AFM micrographs of samples grown at 630 and 430 °C thermocouple temperature. Step-flow growth mode can be achieved for near lattice-matched (9% Sc) samples grown at higher temperatures. As Sc composition and growth temperature increase, the morphology becomes more 3D-dominant and the rms roughness increases.

rms roughnesses were below 0.35 nm. Higher Sc composition and growth temperature induced stronger strain relaxation and promoted the formation of smaller, more three-dimensional islands on the surface, resulting in rms roughnesses above 0.4 nm.

From the Sc composition- and temperature-dependent data described, the optimal growth conditions of lattice-matched AlScN on GaN for multilayer structures are 9%–11% Sc at growth temperatures between 530 and 630 °C. Using the optimized growth conditions of single-layer AlScN/GaN, we grew near lattice-matched multilayer AlScN/GaN heterostructures with 45 nm AlScN/40 nm GaN periods and a targeted 12% Sc composition for structural and transport properties characterization. By using semi-insulating GaN substrates, we were able to measure the total polarization induced mobile charges formed at the AlScN/GaN and GaN/AlScN heterointerfaces. Similar heterostructures grown on conductive $n^+$ GaN substrates have been shown to be promising new lattice-matched GaN-based distributed Bragg reflectors,[10] but the transport properties of AlScN/GaN conductive channels were not reported due to

n-type conductivity of the substrate. A ten period (n = 10) and a twenty period (n = 20) AlScN/GaN (45/40 nm) heterostructure were grown at $T_{sub}$ = 530 °C, as shown in Fig. 5(a). While this growth temperature is 100–150 °C below the optimal growth temperature of GaN in our MBE system, it is more suitable for near lattice-matched AlScN growths, as shown in Fig. 4. The AFM image in Fig. 5(b) shows that step-flow growth mode and clear atomic steps were achieved in both samples, with rms roughness of 0.49 nm for n = 10 and 0.54 nm for the n = 20 (supplementary material, Fig. S1) despite the N-rich growth condition of the AlScN layers and the relatively low growth temperature of the GaN layers.

The RSM shown in Fig. 5(c) reveals that the AlScN layers are nearly strained to the underlying GaN substrate, showing a 0.02% higher in-plane lattice constant compared to GaN. This mismatch is increased to 0.03% for n = 20, suggesting a stronger compressive strain relaxation of AlScN layers, likely due to the Sc composition slightly exceeding the lattice-matched composition (supplementary material, Fig. S1). The well-resolved interference thickness fringes
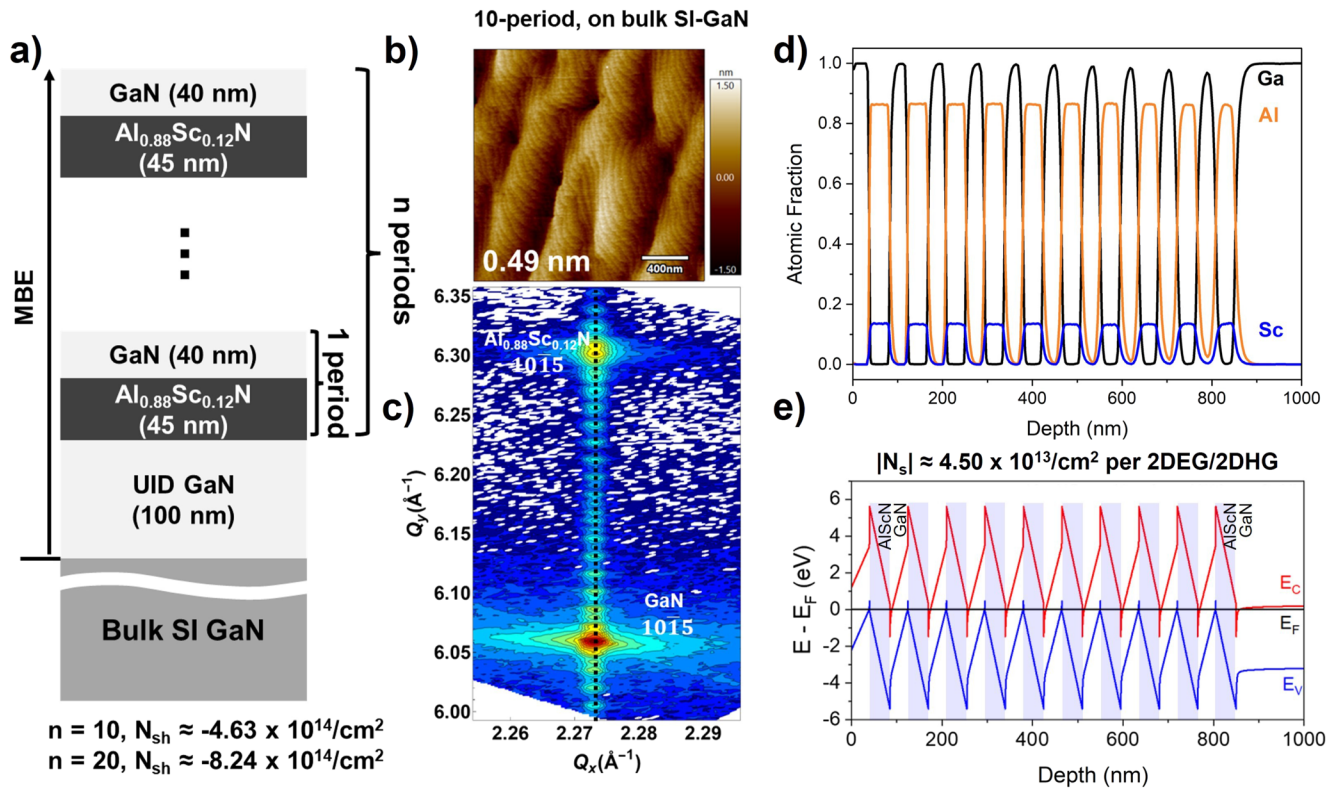


**FIG. 5.** (a) Heterostructure schematics of n-period (n = 10, 20) AlScN/GaN multilayer structures and their corresponding Hall effect measurement sheet carrier densities. (b) $2 \times 2 \ \mu m^2$ AFM micrograph of the ten-period sample shows that step-flow growth mode was maintained even with nitrogen-rich AlScN growth, and a total MBE thickness of nearly 1 $\mu m$; sub-5 Å RMS roughness was achieved, showing the high layer and interface qualities enabled by near lattice-matched growth conditions. Similar surface morphology and roughness were seen on the 20-period sample (supplementary material, Fig. S1). (c) The RSM scan of the ten-period sample shows that all the MBE layers are coherently strained to the bulk GaN substrate; this is enabled by the higher critical AlScN thickness for near lattice-matched Sc compositions. (d) SIMS data of the ten-period sample, showing stable Sc composition (13% ± 1%) was achieved in AlScN layers throughout the heterostructure compared to 12% ± 1.5% measured by EDS. (e) Schrodinger–Poisson 1D simulation of the ten-period heterostructure, showing ten 2DEGs at the AlScN-GaN interfaces and ten 2DHGs at the GaN-AlScN interface with $4.5 \times 10^{13}/cm^2$ sheet charge density per 2DEG or 2DHG. AlScN layers are highlighted in blue stripes. From the experimental sheet charge densities and 1D Poisson simulation, we note that the net experimental sheet charge density scales almost linearly with the number of AlScN/GaN periods.

in RSM scans confirm the high crystalline and interface quality of AlScN and GaN layers. Symmetric $2\theta$-$\omega$ scans of both samples show strong Pendellösung fringes, suggesting sharp interfaces between the AlScN and GaN layers (supplementary material, Fig. S1). In situ RHEED tracking corroborated this, showing streaky RHEED patterns along the $\langle 110 \rangle$ azimuth of AlScN throughout the growth (supplementary material, Fig. S2). The smooth surface morphology with atomic steps and high crystalline and interface quality is enabled by targeting the lattice-matched composition of 11% Sc. XRD fringe simulation of both samples suggests the AlScN and GaN thickness to be 45 and 40 nm (supplementary material, Fig. S1), respectively, agreeing well with the targeted thicknesses.

A strong correlation between the XRD rocking curve (RC) full width at half maximum (FWHM) broadening and strain relaxation due to lattice mismatch was found in previous MBE AlScN studies.[22,33] For n = 10, RC scans about the symmetric [0002] azimuth and asymmetric [$10\bar{1}5$] azimuth of the AlScN peak RC exhibited full width at half maximum FWHM values of 30 arcsec and 30 arcsec, respectively. These low values closely follow the substrate RC FWHMs of 27 and 30 arcsec for the same azimuths (supplementary material, Fig. S3). However, we measured an increase in the [$10\bar{1}5$] azimuth RC FWHM to 48 arcsec for n = 20, corresponding to the increased strain relaxation observed in RSM (supplementary material, Fig. S1). ToF-SIMS data of the ten-period sample shown in Fig. 5(d) demonstrate consistent Sc composition of 13% ± 1% in AlScN layers throughout the heterostructure, agreeing with the 12 ± 1.5% Sc composition measured in both multilayer structures by EDS. The atomic composition tailing between bottom GaN and AlScN layers is likely an artifact of SIMS spatial resolution. This composition is above the lattice-matched composition range, thereby inducing the increased strain relaxation observed from the ten-period to the twenty-period sample. While we clearly observed strain relaxation in 100 nm single-layer AlScN films with Sc composition above 11% (supplementary material, Fig. S1), the critical thickness in a superlattice heterostructure can be four times higher than that of single layers due to the increased resistive force of misfit dislocation formation at new interfaces, resulting in thick

pseudomorphic heterostructures with lattice-mismatched 12% Sc AlScN-GaN epilayers.[40]

Using 1D Poisson,[41] a self-consistent one-dimensional Schrodinger–Poisson solver, the energy band diagram of the ten period AlScN/GaN sample was simulated, as shown in Fig. 5(e). The 1D Poisson simulation predicted 10 two-dimensional electron gases (2DEGs) and 10 two-dimensional hole gases (2DHGs) to form at the AlScN/GaN and GaN/AlScN interfaces, respectively. The absolute carrier density for each 2DEG or 2DHG is $|N_{sh}| = 4.5 \times 10^{13}/\text{cm}^2$. While 2DHGs have not been reported in AlScN/GaN heterostructures, their formation and contribution cannot be experimentally ruled out.

Hall effect measurements at 300 K revealed extremely high mobile electron density in both samples [Fig. 5(a)], with experimental net sheet carrier density $N_{sh} = -4.63 \times 10^{14}/\text{cm}^2$ for n = 10 and $N_{sh} = -8.24 \times 10^{14}/\text{cm}^2$ for n = 20, both of which are the highest values reported in multichannel GaN heterostructures, with less than 6% of the measured net sheet charge density expected to come from n-type conductivity of the unintentionally doped GaN layers. The negative Hall coefficients indicated that the majority of carriers are electrons. By dividing the measured carrier density by the simulated 2DEG density of $4.5 \times 10^{13}/\text{cm}^2$ per channel, we get 10.2 effective 2DEGs for n = 10 and 18.4 effective 2DEGs for n = 20, thereby demonstrating linear scaling of net charge density with the number of AlScN/GaN periods. The electron mobilities measured for n = 10 and n = 20 samples are 14 and 2 $\text{cm}^2/\text{V.s}$, respectively. Since excess Ga was fully desorbed before N-rich AlScN growths, strong interface roughness scattering and alloy scattering are expected in these samples. Interface roughness scattering and alloy scattering have a strong effect on electron mobility at the AlScN-GaN interface,[42] so growth optimization is needed to enhance the sheet charge mobility. In particular, the introduction of an AlN interlayer at each AlScN-GaN interface can help boost the 2DEG mobility.[42] However, AlN and AlScN strain engineering will be needed to maintain the pseudomorphic strain throughout the heterostructure with multiple AlN interlayers. Furthermore, the possible contribution of heavier carriers and lower mobility from 2DHGs could also limit the Hall effect
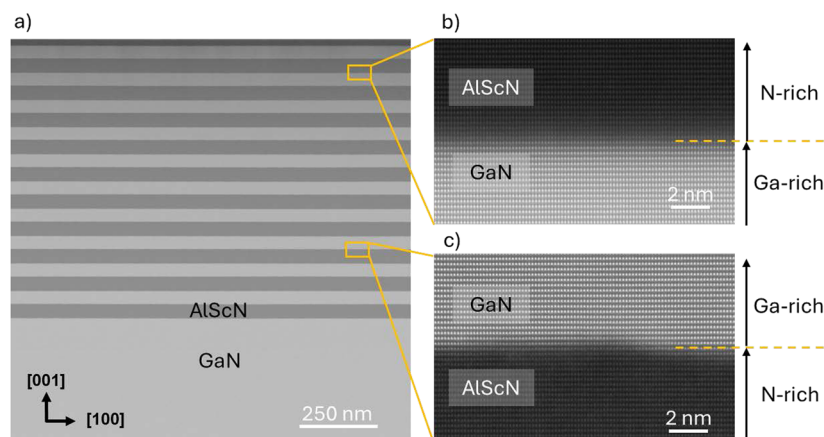


**FIG. 6.** (a) Large field-of-view ADF-STEM image of a 12% Sc AlScN/GaN ten period multilayer structure on a bulk GaN substrate. Panels (b) and (c): atomic resolution ADF-STEM image of representative AlScN/GaN interfaces and associated MBE growth conditions.

24 October 2024 18:28:51

mobility measured in these samples, suggesting the potential need for Si delta doping at the GaN-AlScN interfaces.

Figure 6(a) shows an annular dark-field scanning transmission electron microscopy (ADF-STEM) image showing ten uniform layers of the heterostructure composed of 45 nm thick AlScN with 12% Sc and 40 nm thick GaN. No threading or edge dislocations are visible in this field of view (~1.3 $\mu$m), indicating high-quality epitaxial growth near lattice-matched conditions between AlScN and GaN. In a larger field-of-view ADF image spanning more than 7 $\mu$m, we observed vertical dislocations stemming from the substrate and buffer layer interface. These dislocations contribute to the relaxation of the slight remnant strain present between AlScN and GaN (supplementary material, Fig. S4). The upper bound of in-plane strain calculated based on the average distance between visible dislocations corresponds to 0.02% compressive strain of AlScN epilayers, consistent with the RSM measurements. The interfaces between GaN and AlScN layers were studied by atomic resolution ADF-STEM images. A smooth diffuse AlScN/GaN interface is observed across 3–4 monolayers shown in Fig. 6(b). The gradient in the image contrast describes the change in chemical composition despite our efforts during growth to desorb excess Ga and minimize the Ga incorporation into AlScN. The physical origin of the diffuse interface requires further investigation to minimize the alloy scattering expected to affect the 2DEG. In comparison, Fig. 6(c) shows ~1 nm surface roughness at the GaN/AlScN interface. This interface morphology and roughness are consistent with the surface morphology observed in other AlScN epilayers grown under nitrogen-rich conditions.[24]

We further analyzed the surface layers of the ten period 12% Sc composition AlScN/GaN multilayer sample using phase lock-in analysis.[43] We did not observe in-plane lattice mismatch within the precision of the measurement across an ~80 nm field of view (supplementary material, Fig. S5). The strain variance in AlScN is on the same order as the noise variance in GaN and does not display systematic differences. The AlScN out-of-plane lattice constant matches the $c$ lattice constant of 12% Sc composition AlScN film [Fig. 3(b)]. We, therefore, conclude that the AlScN layers are strained to the same in-plane lattice constant as GaN in the ten-period multilayer heterostructure despite the slight variation from lattice-matched Sc composition.

As a final point of discussion, lattice-matched AlScN/GaN multilayer structures have a bright outlook for future GaN-based electronics, optoelectronics, and photonics. The pseudomorphic nature of lattice-matched epilayers also means that the number of AlScN/GaN periods and AlScN thickness can be flexibly chosen for various multilayer heterostructure engineering. For example, lattice-matched AlScN/GaN distributed Bragg reflectors with AlScN layers thicker than 40 nm can be a new platform for GaN-based bottom DBRs that can outperform the existing AlInN/GaN DBRs.[10] AlScN/GaN multiple quantum wells with AlScN layers thinner than 10 nm are capable of strong near-infrared intersubband absorption (ISBA).[30,44] Similarly, GaN-based heterostructures that require Al(Ga,In)N/GaN multiple quantum wells, such as resonant tunneling diodes, quantum cascade lasers, and multichannel transistors, stand to benefit from the wide bandgap, highly polar lattice-matched AlScN material. The understanding of lattice parameters as a function of alloy composition and growth conditions also provides more general guidance for strain engineering

of AlScN in multilayer,[45] high Sc composition,[46] or compositionally graded[47] heterostructures. It is important to note that while using the same growth technique (MBE), the lattice-matched composition of AlScN in this work and in the works of Dinh *et al.*, Kumar *et al.*, and Dzuba *et al.* are 9%–11%, 9%, 14%, and 18% Sc, respectively.[22,30,33] Therefore, a more comprehensive examination on the effects of growth conditions on the AlScN lattice-matched composition is needed to deliver high-quality pseudomorphic AlScN/GaN multilayer heterostructures.

## IV. CONCLUSION

In summary, new understandings of AlScN/GaN single-layer and multilayer heterostructures were achieved in this work. First, we found that the lattice-matched composition of MBE-grown AlScN on GaN is around 9%–11% Sc. Lattice-matched AlScN films with 9%–11% Sc can be grown using a large temperature window, providing guidance to optimizing the growth conditions and crystal quality of AlScN epilayers and AlScN/GaN multilayer structures. The lower lattice-matched composition here can have important implications for AlScN integration with GaN, such as interplaying strain engineering, high-k dielectric, and ferroelectric properties. Next, near pseudomophic AlScN/GaN multilayer heterostructures with ten and twenty AlScN/GaN periods were realized by MBE. Excellent surface and interface roughness were verified via AFM, XRD, and ADF-STEM analyses. Net mobile electron charge density as high as $8.24 \times 10^{14}$/cm$^2$ for twenty channels and linear carrier density scaling with the number of AlScN/GaN periods was achieved, suggesting the presence of multiple polarization-induced conduction channels enabled by growing near lattice-matched conditions. These results provide a new understanding of AlScN/GaN epitaxial growth by MBE and highlight the benefits of lattice-matched AlScN and lattice-matched AlScN/GaN multilayer heterostructures for multiple quantum well heterostructures in future GaN-based power electronics and photonics.

## SUPPLEMENTARY MATERIAL

See the supplementary material for XRD, AFM, RSM, and XRD rocking curve scans of the ten and twenty period AlScN/GaN samples on bulk semi-insulating GaN substrates, the RHEED patterns of the AlScN during a multilayer growth, the RSM of single layer AlScN films with various Sc compositions, the ADF-STEM image with vertical dislocation stemming from the substrate, and the RBS spectra.

## ACKNOWLEDGMENTS

## AUTHOR DECLARATIONS

### Conflict of Interest

The authors have no conflicts to disclose.

### Author Contributions

**Thai-Son Nguyen**: Conceptualization (lead); Data curation (lead); Formal analysis (lead); Investigation (lead); Methodology (lead); Validation (lead); Writing – original draft (lead); Writing – review & editing (lead). **Naomi Pieczulewski**: Formal analysis (supporting); Investigation (supporting); Methodology (supporting); Validation (supporting); Writing – original draft (supporting); Writing – review & editing (supporting). **Chandrashekhar Savant**: Data curation (supporting); Formal analysis (supporting); Investigation (supporting); Validation (supporting); Writing – original draft (supporting); Writing – review & editing (supporting). **Joshua J. P. Cooper**: Data curation (supporting); Formal analysis (supporting); Investigation (supporting); Methodology (supporting); Validation (supporting); Writing – original draft (supporting); Writing – review & editing (supporting). **Joseph Casamento**: Conceptualization (equal); Validation (equal); Writing – review & editing (equal). **Rachel S. Goldman**: Methodology (supporting); Resources (supporting); Writing – review & editing (supporting). **David A. Muller**: Methodology (supporting); Validation (supporting). **Huili G. Xing**: Funding acquisition (equal); Project administration (supporting); Resources (equal); Supervision (supporting); Writing – review & editing (supporting). **Debdeep Jena**: Conceptualization (equal); Funding acquisition (equal); Investigation (supporting); Methodology (supporting); Project administration (lead); Resources (equal); Supervision (lead); Validation (supporting); Writing – original draft (supporting); Writing – review & editing (supporting).

## DATA AVAILABILITY

The data that support the findings of this study are available from the corresponding author upon reasonable request.

## REFERENCES

[1]M. Akiyama, K. Kano, and A. Teshigahara, "Influence of growth temperature and scandium concentration on piezoelectric response of scandium aluminum nitride alloy thin films," Appl. Phys. Lett. **95**, 162107 (2009).

[2]M. Akiyama, T. Kamohara, K. Kano, A. Teshigahara, Y. Takeuchi, and N. Kawahara, "Enhancement of piezoelectric response in scandium aluminum nitride alloy thin films prepared by Dual Reactive Cosputtering," Adv. Mater. **21**, 593–596 (2009).

[3]S. Fichtner, N. Wolff, F. Lofink, L. Kienle, and B. Wagner, "AlScN: A III–V semiconductor based ferroelectric," J. Appl. Phys. **125**, 114103 (2019).

[4]D. Wang, P. Wang, S. Mondal, S. Mohanty, T. Ma, E. Ahmadi, and Z. Mi, "An epitaxial ferroelectric ScAlN/GaN heterostructure memory," Adv. Electron. Mater. **8**, 2200005 (2022).

[5]X. Zhang, E. A. Stach, W. J. Meng, and A. C. Meng, "Nanoscale compositional segregation in epitaxial AlScN on Si (111)," Nanoscale Horizons **8**, 674–684 (2023).

[6]S. Yasuoka, R. Mizutani, R. Ota, T. Shiraishi, T. Shimizu, M. Uehara, H. Yamada, M. Akiyama, and H. Funakubo, "Tunable ferroelectric properties in wurtzite $Al_{0.8}Sc_{0.2}N$ via crystal anisotropy," ACS Appl. Electron. Mater. **4**, 5165–5170 (2022).

[7]M. Uehara, R. Mizutani, S. Yasuoka, T. Shimizu, H. Yamada, M. Akiyama, and H. Funakubo, "Lower ferroelectric coercive field of ScGaN with equivalent remanent polarization as ScAlN," Appl. Phys. Express **15**, 081003 (2022).

[8]K. D. Kim, Y. B. Lee, S. H. Lee, I. S. Lee, S. K. Ryoo, S. Y. Byun, J. H. Lee, and C. S. Hwang, "Impact of operation voltage and $NH_3$ annealing on the fatigue characteristics of ferroelectric AlScN thin films grown by sputtering," Nanoscale **15**, 16390–16402 (2023).

[9]V. Yoshioka, J. Lu, Z. Tang, J. Jin, R. H. Olsson III, and B. Zhen, "Strongly enhanced second-order optical nonlinearity in CMOS-compatible $Al_{1-x}Sc_xN$ thin films," APL Mater. **9**, 101104 (2021).

[10]L. van Deurzen, T.-S. Nguyen, J. Casamento, H. G. Xing, and D. Jena, "Epitaxial lattice-matched AlScN/GaN distributed Bragg reflectors," Appl. Phys. Lett. **123**, 241104 (2023).

[11]H. Kroemer, "Nobel lecture: Quasielectric fields and band offsets: Teaching electrons new tricks," Rev. Mod. Phys. **73**, 783–793 (2001).

[12]R. S. Howell, B. Novak, T. Vasen, P. Shea, J. Chang, and S. Afroz, "GaN SLCFET technology for next generation mmW systems, demonstrating $P_{out}$ of 10.87 W/mm with 43% PAE at 94 GHz," IEEE Microwave Wireless Technol. Lett. **33**, 839–842 (2023).

[13]J. Faist, F. Capasso, D. L. Sivco, C. Sirtori, A. L. Hutchinson, and A. Y. Cho, "Quantum cascade laser," Science **264**, 553–556 (1994).

[14]A. Kikuchi, R. Bannai, K. Kishino, C.-M. Lee, and J.-I. Chyi, "AlN/GaN double-barrier resonant tunneling diodes grown by RF-plasma-assisted molecular-beam epitaxy," Appl. Phys. Lett. **81**, 1729–1731 (2002).

[15]R. Butté, E. Feltin, J. Dorsaz, G. Christmann, J.-F. Carlin, N. Grandjean, and M. Ilegems, "Recent progress in the growth of highly reflective nitride-based distributed Bragg reflectors and their use in microcavities," Jpn. J. Appl. Phys. **44**, 7207 (2005).

[16]H. Hirayama, W. Terashima, T.-T. Lin, and M. Sasaki, "Recent progress and future prospects of THz quantum-cascade lasers," in *Novel In-Plane Semiconductor Lasers XIV* (SPIE, 2015), Vol. 9382, pp. 157–167.

[17]M. Xiao, Y. Ma, K. Cheng, K. Liu, A. Xie, E. Beam, Y. Cao, and Y. Zhang, "3.3 kV multi-channel AlGaN/GaN Schottky barrier diodes with P-GaN termination," IEEE Electron Device Lett. **41**, 1177–1180 (2020).

[18]A. Terano, T. Tsuchiya, K. Mochizuki, S. Tanaka, and T. Nakamura, "GaN-based multi-two-dimensional-electron-gas-channel diodes on sapphire substrates with breakdown voltage of over 3 kV," Jpn. J. Appl. Phys. **54**, 066503 (2015).

[19]K. E. Waldrip, J. Han, J. J. Figiel, H. Zhou, E. Makarona, and A. V. Nurmikko, "Stress engineering during metalorganic chemical vapor deposition of AlGaN/GaN distributed Bragg reflectors," Appl. Phys. Lett. **78**, 3205–3207 (2001).

[20]G. S. Huang, T. C. Lu, H. H. Yao, H. C. Kuo, S. C. Wang, C.-W. Lin, and L. Chang, "Crack-free GaN/AlN distributed Bragg reflectors incorporated with GaN/AlN superlattices grown by metalorganic chemical vapor deposition," Appl. Phys. Lett. **88**, 061904 (2006).

[21]M. A. Moram and S. Zhang, "ScGaN and ScAlN: Emerging nitride materials," J. Mater. Chem. A **2**, 6042–6050 (2014).

[22]D. V. Dinh, J. Lähnemann, L. Geelhaar, and O. Brandt, "Lattice parameters of $Sc_xAl_{1-x}N$ layers grown on GaN(0001) by plasma-assisted molecular beam epitaxy," Appl. Phys. Lett. **122**, 152103 (2023).

[23] R. Deng, S. R. Evans, and D. Gall, "Bandgap in $Al_{1-x}Sc_xN$," Appl. Phys. Lett. **102**, 112103 (2013).

[24] M. T. Hardy, E. N. Jin, N. Nepal, D. S. Katzer, B. P. Downey, V. J. Gokhale, D. F. Storm, and D. J. Meyer, "Control of phase purity in high scandium fraction heteroepitaxial ScAlN grown by molecular beam epitaxy," Appl. Phys. Express **13**, 065509 (2020).

[25] J. Casamento, C. S. Chang, Y.-T. Shao, J. Wright, D. A. Muller, H. G. Xing, and D. Jena, "Structural and piezoelectric properties of ultra-thin $Sc_xAl_{1-x}N$ films grown on GaN by molecular beam epitaxy," Appl. Phys. Lett. **117**, 112101 (2020).

[26] P. Wang, D. A. Laleyan, A. Pandey, Y. Sun, and Z. Mi, "Molecular beam epitaxy and characterization of wurtzite $Sc_xAl_{1-x}N$," Appl. Phys. Lett. **116**, 151903 (2020).

[27] K. Motoki, Z. Engel, T. M. McCrone, H. Chung, C. M. Matthews, S. Lee, E. N. Marshall, A. Ghosh, A. Tang, and W. A. Doolittle, "Improved crystallographic order of ScAlN/GaN heterostructures grown at low temperatures under metal rich surface conditions," J. Appl. Phys. **135**, 135105 (2024).

[28] O. Ambacher, S. Mihalic, M. Yassine, A. Yassine, N. Afshar, and B. Christian, "Review: Structural, elastic, and thermodynamic properties of cubic and hexagonal $Sc_xAl_{1-x}N$ crystals," J. Appl. Phys. **134**, 160702 (2023).

[29] T. Maeda, Y. Wakamoto, S. Kaneki, H. Fujikura, and A. Kobayashi, "Structural and optical properties of epitaxial $Sc_xAl_{1-x}N$ coherently grown on GaN bulk substrates by sputtering method," Appl. Phys. Lett. **125**, 022103 (2024).

[30] B. Dzuba, T. Nguyen, A. Sen, R. E. Diaz, M. Dubey, M. Bachhav, J. P. Wharry, M. J. Manfra, and O. Malis, "Elimination of remnant phases in low-temperature growth of wurtzite ScAlN by molecular-beam epitaxy," J. Appl. Phys. **132**, 175701 (2022).

[31] C. Höglund, J. Birch, B. Alling, J. Bareño, Z. Czigány, P. O. Persson, G. Wingqvist, A. Zukauskaite, and L. Hultman, "Wurtzite structure $Sc_xAl_{1-x}N$ solid solution films grown by reactive magnetron sputter epitaxy: Structural characterization and first-principles calculations," J. Appl. Phys. **107**, 123515 (2010).

[32] R. Dargis, A. Clark, A. Ansari, Z. Hao, M. Park, D. Kim, R. Yanka, R. Hammond, M. Debnath, and R. Pelzel, "Single-crystal multilayer nitride, metal, and oxide structures on engineered silicon for new-generation radio frequency filter applications," Physica Status Solidi A **217**, 1900813 (2020).

[33] R. Kumar, G. Gopakumar, Z. U. Abdin, M. J. Manfra, and O. Malis, "Pinpointing lattice-matched conditions for wurtzite $Sc_xAl_{1-x}N$/GaN heterostructures with x-ray reciprocal space analysis," Appl. Phys. Lett. **125**, 052103 (2024).

[34] M. T. Hardy, B. P. Downey, N. Nepal, D. F. Storm, D. S. Katzer, and D. J. Meyer, "Epitaxial ScAlN grown by molecular beam epitaxy on GaN and SiC substrates," Appl. Phys. Lett. **110**, 162104 (2017).

[35] S. Zhang, W. Y. Fu, D. Holec, C. J. Humphreys, and M. A. Moram, "Elastic constants and critical thicknesses of ScGaN and ScAlN," J. Appl. Phys. **114**, 243516 (2013).

[36] D. F. Urban, O. Ambacher, and C. Elsässer, "First-principles calculation of electroacoustic properties of wurtzite (Al,Sc)N," Phys. Rev. B **103**, 115204 (2021).

[37] I. Bryan, Z. Bryan, M. Bobea, L. Hussey, R. Kirste, R. Collazo, and Z. Sitar, "Homoepitaxial AlN thin films deposited on m-plane (1-100) AlN substrates by metalorganic chemical vapor deposition," J. Appl. Phys. **116**, 133517 (2014).

[38] S. Yasuoka, T. Shimizu, A. Tateyama, M. Uehara, H. Yamada, M. Akiyama, and H. Funakubo, "Impact of deposition temperature on crystal structure and ferroelectric properties of $Al_{1-x}Sc_xN$ films prepared by sputtering method," Physica Status Solidi A **218**, 2100302 (2021).

[39] S. Ndiaye, C. Elias, A. Diagne, H. Rotella, F. Georgi, M. Hugues, Y. Cordier, F. Vurpillot, and L. Rigutti, "Alloy distribution and compositional metrology of epitaxial ScAlN by atom probe tomography," Appl. Phys. Lett. **123**, 162102 (2023).

[40] J. W. Matthews and A. E. Blakeslee, "Defects in epitaxial multilayers: I. Misfit dislocations," J. Cryst. Growth **27**, 118–125 (1974).

[41] G. Snider, 1D Poisson solver, available at https://www3.nd.edu/gsnider/.

[42] J. Casamento, T.-S. Nguyen, Y. Cho, C. Savant, T. Vasen, S. Afroz, D. Hannan, H. G. Xing, and D. Jena, "Transport properties of polarization-induced 2D electron gases in epitaxial AlScN/GaN heterojunctions," Appl. Phys. Lett. **121**, 192101 (2022).

[43] B. H. Goodge, I. El Baggari, S. S. Hong, Z. Wang, D. G. Schlom, H. Y. Hwang, and L. F. Kourkoutis, "Disentangling coexisting structural order through phase lock-in analysis of atomic-resolution STEM data," Microsc. Microanal. **28**, 404–411 (2022).

[44] G. Gopakumar, Z. U. Abdin, R. Kumar, B. Dzuba, T. Nguyen, M. J. Manfra, and O. Malis, "Conduction-band engineering of polar nitride semiconductors with wurtzite ScAlN for near-infrared photonic devices," J. Appl. Phys. **135**, 165701 (2024).

[45] J. X. Zheng, D. Wang, P. Musavigharavi, M. M. A. Fiagbenu, D. Jariwala, E. A. Stach, and R. H. Olsson III, "Electrical breakdown strength enhancement in aluminum scandium nitride through a compositionally modulated periodic multilayer structure," J. Appl. Phys. **130**, 144101 (2021).

[46] M. T. Hardy, A. C. Lang, E. N. Jin, N. Nepal, B. P. Downey, V. J. Gokhale, D. Scott Katzer, and V. D. Wheeler, "Nucleation control of high crystal quality heteroepitaxial $Sc_{0.4}Al_{0.6}N$ grown by molecular beam epitaxy," J. Appl. Phys. **134**, 105301 (2023).

[47] J. Simon, V. Protasenko, C. Lian, H. Xing, and D. Jena, "Polarization-induced hole doping in wide–band-gap uniaxial semiconductor heterostructures," Science **327**, 60–64 (2010).